Small scale experimental validation of a numerical model of the HarshLab2.0 floating platform coupled with a non-linear lumped mass catenary mooring system

Imanol Touzon[1,2], Vincenzo Nava[1,3], Zhen Gao[4], Iñigo Mendikoa[1], Victor Petuya[2]

[1] Tecnalia Research & Innovation, Offshore Renewable Energy Area

[2] Department of Mechanical Engineering – University of the Basque Country - UPV/EHU

[3] Basque Centre for Applied Mathematics, BCAM; Bilbao, Spain

[4] Department of Marine Technology - Norwegian University of Science and Technology - NTNU

Abstract

When focusing on mooring system numerical modelling, the efforts are focused on validating models that increase the accuracy and maintain the computation time under reasonable limits. In this paper an approach for modelling the interaction among supporting structure and mooring system is introduced through kinematic relations. The proposed approach has been validated with the experimental wave tank 1:13.6 scaled data of the HarshLab 2.0 platform, a CALM type buoy moored with a three-line catenary system and used as a floating laboratory for materials and corrosion testing, to be installed at BiMEP. The drag forces of the buoy as well as the Morison coefficients of the heave-pitch coupling, induced by the attached structure for ships bow landing, have been identified. Results of the mooring line tensions are validated with imposed displacements of the structure and, subsequently, with coupled simulations of the moored buoy in a set of realistic sea states. Sources of differences on the estimation of line tensions are found to be mainly due to uncertainties of seabed friction forces, a high sensitivity of line tensions to small swaying and a poor pitching performance of the numerical model, very likely due to a very non-linear pitching of the physical model.

Keywords

Catenary Mooring System, Linear Hydrodynamics, Lumped mass, Lagrange Multipliers, Offshore Renewable Energy

1 Introduction

Catenary mooring systems are strongly nonlinear and can be simulated with nonlinear time domain numerical models, accounting for non-linearities, e.g. nonlinear geometric stiffness and the drag term. The dynamic nonlinear time domain lumped mass method for mooring system modelling consists in modelling mooring lines as mass points connected to adjacent points by spring and dampers, which represent internal structural characteristics of the line material.

Main author: Imanol Touzon

e-mail address: imanol.touzon@tecnalia.com

Postal address: Parque Tecnológico de Bizkaia, Astondo Bidea, Edificio 700,E-48160 Derio - Bizkaia (Spain)

Declarations of interest: none

This method is widely used in the offshore industry since initially introduced by Van den Boom [1]. It has been applied within the offshore renewable energy sector by [2] as well as the non-linear finite element method (FEM) by [3]among others. Both show accurate line tension results with imposed motions and regular waves and highlight the poor tension estimation of the quasi static (QS) time domain approach. In [2] it is also stated that structure hydrodynamics seem to introduce larger uncertainty than the lumped mass mooring model, however structure motions are not significantly sensitive to using either the QS or the coupled lumped mass models. Reference [4] used a non-linear FEM coupled with linear potential coefficients in a commercial code and points at significant improvements of line tension estimates using full QTFs instead of the Newman approximation. It has also been verified in [5]that full QTF provides better results in terms of mooring line tensions, especially in shallow waters. Linear potential methods are widely accepted in offshore renewable engineering practice, as shown in [2], [4] or [6] for numerical modelling of wave structure interactions. Obtained hydrodynamic coefficients are commonly complemented with a non-linear viscous drag term within certain limits of the Keulegan Carpenter (KC) number. References [4] and [6] applied different numerical fitting methods to compute the additional damping, both used data obtained from the decay tests of their corresponding physical models. Yet, [6] points at some uncertainty in the pitching excitation force estimates as well as the influence of the fitted drag force on the coupled results.

The coupling scheme in [2] and [7] is carried out through parallel numerical models, sharing forces and motions between the structure and the mooring models, and the same scheme is adopted by the commercial code DNVGL-Sesam [8] [9]. Other codes, such as Orcaflex [10], include stiffness and damping terms directly between the corresponding degrees of freedom to model line connections to the seabed and the floating structure. This scheme has also been presented in [11] which allows both mechanical systems to be solved fully coupled.

In the present paper linear hydrodynamics, complemented with fitted viscous force in all degrees of freedom and Morison force for heave and pitch coupling effects, of the floating structure and second order wave drift forces based on Newman approximation have been coupled with a lumped mass model for the mooring system. The lumped mass model considers the inertia and hydrodynamic Morison forces on mooring lines as well as seabed interaction and gravity forces. the mooring-structure coupling has been carried out in a systematic manner imposing kinematic relations on the fairleads, adding mass, damping and stiffness matrices, which enables the resolution of both numerical models integrated into a single one. The main advantage of the herein introduced model is that once the natural frequency and critical damping of the connections are set, the kinematic relations between the degrees of freedom to be connected can be defined in a simplified and a systematic manner and that the coupled system can be solved either in the time or frequency domain.

Such a model has been validated with experimental wave tank testing of the HarshLab 2.0 platform and it is here presented. The HarshLab 2.0 platform is designed to be a floating laboratory off the Basque country coast, at bimep [12], to test in a real environment a variety of offshore materials [13]. The validation is based on decay tests of the floating structure without mooring lines for the degrees of freedom with hydrostatic stiffness (heave, pitch and roll) and with mooring lines for the degrees of freedom without it (surge, sway and yaw). Additionally, irregular waves are simulated in a first step with imposed motions to the floater in the numerical

model and later with the hydrodynamics coupled to mooring dynamics with good agreement with the experiments. Main uncertainties have been found in the mooring lines with transverse motions and in the pitching motion, very likely due to a very non-linear performance. The latter has already been observed in [4] and [6] . Such floater and mooring coupled models can be relevant for small displacement structures such as floating wave energy or floating offshore wind since the coupling effect between both systems may be significant.

2 Numerical model

The hydrodynamic interaction of the herein developed numerical model is based on the linear potential hydrodynamics and Boundary Integral Element Method (BIEM), implemented in codes such as WAMIT [14], ANSYS-AQWA [15] or Nemoh [16]. The dynamic mooring system is based on a lumped mass method in which for each line the hydrodynamics, seabed interaction, gravity and inertia forces are computed. Lines are linked to the floating structure and to the anchor points through imposed kinematic relations by means of Lagrange multipliers making use of the penalty method, as described in [17]. All systems together can be reduced to a collection of mass, damping and stiffness matrices which, along with nonlinear forces, are integrated and updated in the time domain as described below.

Drag forces in the degrees of freedom with hydrostatic stiffness have been identified with the hydrodynamic numerical model without mooring system while in the degrees of freedom without hydrostatics the same model coupled with the mooring system has been applied. The dynamic mooring model isolated from the structure has been validated imposing the motions obtained in the physical testing and being compared with the corresponding line tensions. Finally, the coupled numerical model has been simulated to be compared with both structure motions and lines tensions obtained in the tank tests.

Floating structure hydrodynamics

Floating structure is modelled through linear hydrodynamics as per equation (1). Its interaction with sea waves is summarized through the added mass (A), radiation damping (B), hydrostatic stiffness (H) and Forude Krilov and diffraction force (F_{fk}). Its formulation in the time domain was introduced by W.E. Cummins [18] and described in [19]:

$$(1)\quad [M + A_\infty] \cdot \{\ddot{\delta}(t)\} + \left\{\int_{-\infty}^{t} B(t-\tau) \cdot \dot{\delta}(\tau) \cdot d\tau\right\} + [H] \cdot \{\delta(t)\} = \{F_{fk}(t)\} + \{F^{sv}(t)\}$$

Where square brackets [ ] indicate a matrix and curly brackets { } indicate a vector. Each variable is described below:

- M: Mass matrix of the floater
- A_∞: Added mass at infinite frequency
- $B(t-\tau)$: Radiation impulse response function
- H: Hydrostatic stiffness
- $\delta(t)$; $\dot{\delta}(t)$; $\ddot{\delta}(t)$: Floater rigid body motions
- $F_{fk}(t)$: Froude Krilov and diffraction force

- $F^{sv}(t)$: Slowly varying second order drift force

The convolution integral is solved in the time domain by means of direct integration at each time step. To do so, a variable time length has been selected for the radiation impulse response function (RIRF) of each degree of freedom. This length is based on the decay rate of the function maxima, considering an amplitude difference of less than 1% between two successive peaks. This approach has been proven to be coherent with other numerical models as verified in [20] and [21].

Slow drift excitation loads

Slow drift excitation loads have been applied as derived in [19]. The general expression consists of a double summation of the second-order difference frequency loads:

$$(2)\quad F_i^{SV}(t) = \sum_{j=1}^{N}\sum_{k=1}^{N} A_j \cdot A_k \cdot \left[T_{jk}^{ic} \cdot cos\{(\omega_k - \omega_j)\cdot t + (\varphi_k - \varphi_j)\} + T_{jk}^{is} \cdot sin\{(\omega_k - \omega_j)\cdot t + (\varphi_k - \varphi_j)\}\right]$$

Where:

- N: total number of frequencies
- A: Wave amplitude of the frequency component
- T: Quadratic transfer function
- ω: Frequency
- φ: Phase

The main diagonal of $[T]$ has been computed with mentioned linear hydrodynamics codes while off diagonal values have been obtained through the Newman's approximation [19].

Mooring lumped mass model

Lines are modelled as lumped masses, representing adjacent half sections' mass, connected by massless springs and dampers. The reference coordinate system for all bodies to be integrated in time is the global origin (0,0,0), which applies both for the structure and the mooring point masses. Each point mass is made up of 3 degrees of freedom (dof), translational in each of the global directions 'x', 'y' and 'z'. The mechanical system defined by each mooring line can be summarized as in equation (3):

$$(3)\quad [M]\cdot\{\ddot{\delta}(t)\} = \{F(t)\} = \{F_n(t) + F_z(t) + F_f(t) + F_g + F_b + F_{hyd}(t)\}$$

Where:

- $F_n(t)$: Structural stiffness and damping force
- $F_z(t)$: Seabed vertical reaction force
- $F_f(t)$: Seabed horizontal friction force
- F_g: Gravity force
- F_b: Buoyancy force

- $F_{hyd}(\mathrm{t})$: Hydrodynamic Morison force

The massless springs and dampers, connecting point masses, represent axial structural properties of lines. Stiffness and damping forces on each node are represented by forces of the adjacent sections as:

$$(4)\quad F_n = {F_n}^{n+1} - {F_n}^{n-1}$$

Where:

$$(5)\quad {F_n}^{n+1} = \frac{E \cdot A}{{L_0}_n{}^{n+1}} \cdot \frac{1}{{L_n}^{n+1}} \cdot \begin{bmatrix} I_3 & -I_3 \\ -I_3 & I_3 \end{bmatrix} \cdot \begin{Bmatrix} \delta_n \\ \delta_{n+1} \end{Bmatrix} + \left[{C_G}_n{}^{n+1}\right] \cdot \begin{Bmatrix} \dot{\delta}_n \\ \dot{\delta}_{n+1} \end{Bmatrix}$$

$$(6)\quad {C_G}_n{}^{n+1} = \begin{bmatrix} {[R]_n}^{n+1} & 0 \\ 0 & -{[R]_n}^{n+1} \end{bmatrix} \begin{bmatrix} {[C_L]_n}^{n+1} & 0 \\ 0 & -{[C_L]_n}^{n+1} \end{bmatrix} \cdot \begin{bmatrix} {[R]^t}_n{}^{n+1} & 0 \\ 0 & -{[R]^t}_n{}^{n+1} \end{bmatrix}$$

$$(7)\quad {[C_L]_n}^{n+1} = \begin{bmatrix} \beta \cdot \frac{E \cdot A}{{L_0}_n{}^{n+1}} & 0 & 0 \\ 0 & 0 & 0 \\ 0 & 0 & 0 \end{bmatrix}$$

Where:

- sub-index: node ‘n’ in which force ‘F’ is applied
- upper-index: node to which the force ‘F’ connects sub-index node
- C: Damping matrix
- R: Rotation matrix from local to global coordinates
- E: Young elasticity modulus of line material
- A: Cross sectional area of the line
- β: Rayleigh coefficient for structural damping estimation
- L: Deformed section length
- L_0: Undeformed section length
- I_3: Identity matrix of dimension 3

Stiffness and damping matrices account for axial forces and therefore a coordinate system rotation is to be done. To avoid angle determination with sine and cosine computations use of quaternions has been made both for structural damping and Morison forces, as explained in [22] where the quaternion is defined as:

$$(8)\quad [Q]^i = \left[cos\frac{\varphi}{2} \quad a_x \cdot cos\frac{\varphi}{2} \quad a_y \cdot cos\frac{\varphi}{2} \quad a_z \cdot cos\frac{\varphi}{2}\right]^{-1}$$

Where:

- φ: Angle of rotation between initial and final position
- a: Vector defining the rotation axis

The vector defining the rotation between local and global vectors is a perpendicular vector to the plane defined by the local (x_{1L}) and global ($x_{n+1} - x_n$) vectors. The local coordinate system is supposed to be located with the x coordinate aligned with the axis connecting both nodes and positive from the seabed to the structure.

Internal forces are computed for every section of all lines as showed in equation (4) to (7). Having defined lines through their three translational dofs the mass matrix is diagonal, whose values account for adjacent half-length masses. The boundary conditions of the mooring lines are defined by the kinematic relations, as represented in equations (13) to (19).

Through the axial properties of the material, lines geometry and the rotation matrix, the modeled system can be summarized as in Figure 1:

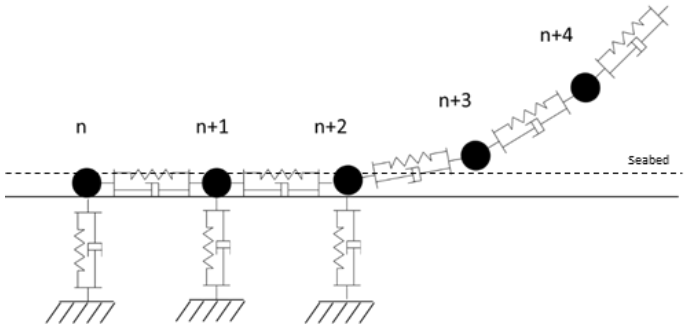

Figure 1 Numerical model forces representation on line nodes

Vertical seabed forces are computed as vertical stiffness and damping forces on the nodes at the seabed. Depending on seabed stiffness, nodes static position will be found deeper in the seabed.

Vertical force is defined as a 1 dof system in which the critical damping and natural frequency are settings of the numerical model:

$$(9)\quad F_z(t) = m_n \cdot \left(\ddot{\delta}_z(t) + 2\xi_v\omega_v\dot{\delta}_z(t) + {\omega_v}^2\delta_z(t)\right)$$

Where:

- ω_v: Vertical natural frequency of seabed nodes
- ξ_v: vertical critical damping of seabed nodes
- δ_z: Vertical motion of each node on the seabed
- m_n: Nodal mass of the 'n^{th}' node

Seabed friction model is implemented through a comparison of total force on the n^{th} node and the corresponding friction force. The force is applied through a damping coefficient, linear up to the total friction force, and kept constant for large velocities, as represented in Figure 2.

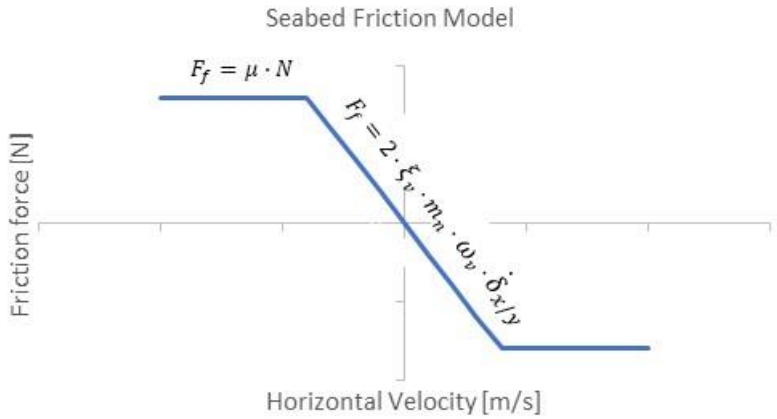

Figure 2 Friction force model

Mooring line external forces

External forces applied on mooring line sections are gravity, buoyancy and hydrodynamic loads. Gravity force is a constant vertical force due to the gravity acceleration over the length assigned to each node:

$$(10)\{F_g\}^n = \begin{Bmatrix} 0 \\ 0 \\ -m \cdot g \end{Bmatrix}$$

Buoyancy force is considered as opposed to the gravity force due to the weight of the water volume displaced (V) by the associated line length (L_n) to each point mass, where ρ_w is the water density:

$$(11)\{F_b\}^n = \begin{Bmatrix} 0 \\ 0 \\ V \cdot \rho_w \cdot g \end{Bmatrix}$$

Hydrodynamic forces on line sections have been accounted for through the Morison equation [19], derived for slender bodies submerged in water:

$$(12)F_{hyd}(t) = (1 + C_a) \cdot \rho_w \cdot V \cdot \dot{u}(t) - C_a \cdot \rho_w \cdot V \cdot \dot{v}(t) + 0.5 \cdot \rho_w \cdot C_d \cdot D \cdot L_n \cdot |u(t) - v(t)| \cdot \big(u(t) - v(t)\big)$$

Where:

- $\dot{u}(\mathrm{t})\ and\ u(\mathrm{t})$: Local acceleration and velocity of fluid particles at each line node
- $\dot{v}(\mathrm{t})\ and\ v(\mathrm{t})$: Local acceleration and velocity of each line node
- D: Diameter of the associated line length

However, velocities used are those in the local coordinate system, radial and axial velocities to line sections. Therefore, node velocities are to be rotated so that the hydrodynamic force can be computed and rotated back into global coordinates. Consequently, the version for inclined cylinders is applied in the model, specified in [19] and [23].

Transfer functions are computed for each node so that water particle dynamics can be computed together with the linear hydrodynamic forces on the structure.

The added mass term is computed as two independent forces, by means of an excitation force and a linear mass matrix as represented by the first two terms of the right-hand side of equation (12). However, the drag term is inherently nonlinear and is computed every time step for every section.

Line attachments

Fairleads and anchor points have been defined by means of multibody relations [17]. It is based on Lagrangian mechanics from which the newton second law can be derived.

Within multibody analysis a widely extended approach is that of Lagrange multipliers. It consists in adding a force term to fulfil the imposed restrictions. Using the penalty method, one obtains the expression (13):

$$(13)\,[M]\cdot\{\ddot{\delta}\}+\left[\Phi_q^T\right]\cdot\alpha_{att}\cdot\left(\left[\ddot{\Phi}(t)\right]+2\xi_{att}\omega_{att}\left[\dot{\Phi}(t)\right]+{\omega_{att}}^2[\Phi(t)]\right)=\{F(t)\}$$

Where Φ_q is the derivative of $\Phi(t)$ with respect to dependent variables, as represented in equation (14):

$$(14)\,\Phi_q=\begin{bmatrix}\frac{\partial\Phi_{11}}{\partial\delta_1} & \cdots & \frac{\partial\Phi_{1n}}{\partial\delta_n}\\ \vdots & \ddots & \vdots\\ \frac{\partial\Phi_{m1}}{\partial\delta_1} & \cdots & \frac{\partial\Phi_{mn}}{\partial\delta_n}\end{bmatrix}$$

It consists in introducing a one degree of freedom mechanical system by kinematic condition with a large natural frequency and inertia. This method introduces forces large enough to maintain the given restrictions with low error rate [17].

Looking at the restriction forces:

- $\Phi(t)=f\left(\delta(t)\right)$: Vector of restrictions
- $\dot{\Phi}(t)$: Derivative with respect to time of the restrictions
- $\ddot{\Phi}(t)$: Second derivative of restriction vector
- ω_{att}: Numerical natural frequency of the attachment force
- ξ_{att}: Numerical critical damping of the attachment force
- α_{att}: Penalizer to make kinematic relation be fulfilled

To compute the restriction forces it is recommended that a very large penalizer is selected in order to obtain the lowest error. However, very large penalizers produce numerical ill-conditioning and it is generally suggested to use factors of 10^7 times the largest term of the mass matrix. Since the nodes of the discretized system tend to be of the order of some kilograms the penalizer has been set to $\alpha_{att}=10\text{^}7$, the natural frequency to be out of the range of the waves excitation $\omega_{att}=10$ and to be critically damped, $\xi_{att}=1$.

Looking at the dependence of the restrictions on the degrees of freedom can be derived its velocity and acceleration:

$$(15)\,\dot{\Phi}(t)=\frac{\partial\Phi(t)}{\partial q}\cdot\dot{\delta}(t)=\Phi_q\cdot\dot{\delta}(t)$$

$$(16)\ddot{\Phi}(t) = \dot{\Phi}_q \cdot \dot{\delta}(t) + \Phi_q \cdot \ddot{\delta}(t)$$

And substituting it yields:

$$(17)\left[M + \alpha\Phi_q^T\Phi_q\right] \cdot \left\{\ddot{\delta}(t)\right\} = \{F(t)\} - \left\{\alpha_{att} \cdot \Phi_q^T \cdot \left(\dot{\Phi}_q \cdot \dot{\delta}(t) + 2\xi_{att}\omega_{att}\Phi_q \cdot \dot{\delta}(t) + {\omega_{att}}^2\Phi(t)\right)\right\}$$

Restrictions for these points are defined as following:

- Fairlead (dynamics of the fairlead of the structure imposed to the mass point 'n'):

$$(18)\Phi = \begin{Bmatrix} x_{est} + x_{roll} + x_{yaw} + \delta_{x-fair} - x_n \\ y_{est} + y_{pitch} + y_{yaw} + \delta_{y-fair} - y_n \\ z_{est} + z_{roll} + z_{pitch} + \delta_{z-fair} - z_n \end{Bmatrix}$$

- Anchor (the mass point '1' of the line must be kept constant at its predefined point):

$$(19)\Phi = \begin{Bmatrix} \delta_{x-anchor} - x_1 \\ \delta_{y-anchor} - y_1 \\ \delta_{z-anchor} - z_1 \end{Bmatrix}$$

Relations presented above have constant derivatives which make them linear and can, therefore, be reduced to a set of stiffness, mass and damping matrices representing the attachment forces plus a set of constant vectors arising from the constant distances δ_{fair} and δ_{anchor}. However, the spatial positions of the fairleads, which involve all terms of equation (18), are dependent on structure rotations and require updating at each time step of such matrices in order to fulfill the imposed restrictions.

Coupled system to be solved

The hydrodynamic and mooring coupled system to be solved can be summarized through a set of mass, damping and stiffness matrices together with a force vector as in equation (20):

$$(20)\begin{bmatrix} (M+A)_{str} & M_{f/a} \\ M_{f/a} & M_{moor} \end{bmatrix} \cdot \begin{Bmatrix} \ddot{\delta}_{str}(t) \\ \ddot{\delta}_{moor}(t) \end{Bmatrix} + \begin{bmatrix} 0 & C_{f/a} \\ C_{f/a} & C_{moor} \end{bmatrix} \cdot \begin{Bmatrix} \dot{\delta}_{str}(t) \\ \dot{\delta}_{moor}(t) \end{Bmatrix} + \begin{bmatrix} H_{str} & K_{f/a} \\ K_{f/a} & K_{moor} \end{bmatrix} \cdot \begin{Bmatrix} \delta_{str}(t) \\ \delta_{moor}(t) \end{Bmatrix} =$$

$$\begin{Bmatrix} F_{fk}(t) + F^{sv}(t) + F_{drag}(t) + F_{bl}(t) - F_{conv}(t) + F_{f/a}(t) \\ \{F_n(t) + F_z(t) + F_f(t) + F_g + F_b + F_{hyd}(t) + F_{f/a}(t)\} \end{Bmatrix}$$

In the equation (20) sub-indexes 'str', 'f/a', 'bl' and 'moor' denote structure, fairleads/anchors, bow landing and mooring respectively. In the structure force vector a non-linear viscous drag term has been added, modelled as the last term of the right-hand side of equation (12). Due to the differences in natural frequencies of the coupled system, equation (20) represents a stiff system and the implicit Newmark integration scheme has been chosen to carry out the integration [24], with a time step of 1e-3s.

3 Physical Model description

Floating Structure

HarshLab 2.0 platform shape is being designed by the consortium made up for its commercial exploitation, as well as its mooring system and the experimental testing has been carried out at the CEHIPAR wave tank. The work here presented aims at characterizing

its hydromechanics both with and without mooring system. The floater is made of a single floating structure, consisting of two vertical cylinders. The larger cylinder is partially submerged, and the freeboard is made up of the remaining part of the structure, as showed in Figure 3 and Figure 4:

Harsh 2.0 buoy shape		
Scale	**1:1**	**1:13.6**
Lower Diameter [m]	10.47	0.77
Lower Height [m]	3.54	0.26
Upper Diameter [m]	5.03	0.37
Upper Height [m]	4.76	0.35
Draft [m]	2.28	0.17
KG [m]	1.67	0.12
Water Depth [m]	68.00	5.00
Total mass [kg]	1.91E+05	76.02
Ixx [kg·m^2]	2.84E+06	6.11
Iyy [kg·m^2]	2.86E+06	6.14
Izz [kg·m^2]	2.75E+06	5.91

Figure 3 Harsh 2.0 platform shape (1:13.6 scale) and its main properties

The model incorporates an attached structure to reproduce the bow landing, as shown in Figure 4, it has an impact on the hydrostatic stiffness and the added viscous damping in all degrees of freedom as summarized in Table 7 and Table 8 respectively. Due to its position it introduces a coupling effect between pitch-heave motions as well as in sway-yaw. The pitch-heave coupling effect, introduced in Figure 9, has been fitted with the obtained coefficients in forced oscillatory tests. However, the yaw-sway coupling effect has not been considered in the numerical model since all tests were performed in the direction defined in Figure 7 and none of them is to be significantly excited.

Figure 4 Experimental physical moored model subject to the sea state 10 as defined in Table 6, side view, (left) and bow landing upper view (right)

Water surface elevation has been measured with two wave sensors, denoted by SB and FO, placed as indicated in Figure 7. The actual water surface elevation on the buoy has been estimated from the SB sensor since it is closer to the structure. Derived phases of the spectra have been corrected to account for the corresponding distance to the structure, by means of the dispersion relation for deep waters [19]. Differences observed in the surface elevation, as shown in Figure 5, obtained with both corrected spectra are lower than 1% in standard deviation, it has been assumed to be low enough to consider a low influence of diffraction and radiation.

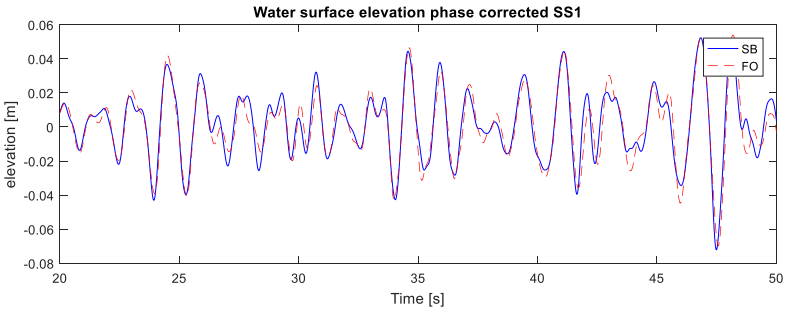

Figure 5 Estimated water surface elevation at the structure position from the sensors available FO and SB

The measures of all variables were gathered in real time with a PC and a sampling frequency of 100Hz, except the pressure gauges that were sampled with 9600Hz. For the variables used in the work here introduced different kind of gauges were used as represented in Figure 6.

- Wave elevation gauges: Two capacitive sensors placed with respect to the structure as shown in Figure 7
- Motion sensors: An optical measurement system was used (KRYPTON) which collected the six degrees of freedom of the structure
- Mooring line tension gauges: Load cells were used both in the fairleads and in the anchoring points of each line
- Forces on the structure: The force on the structure due to its forced motion as well as the mooring force in the stiffness tests a dynamometer JP-MK2 was used

Figure 6 Six degree of freedom dynamometer (left) and load cells for line tension measurement (centre) and a wave elevation gauge (right)

Mooring System

The mooring system is made up of three catenary chain lines with a non-dimensional pretension, as defined in [25], of 1.21[-] for the two front lines (lines 1 and 2) and 1.39[-] for the line at the back (line 3), as defined in Figure 7.

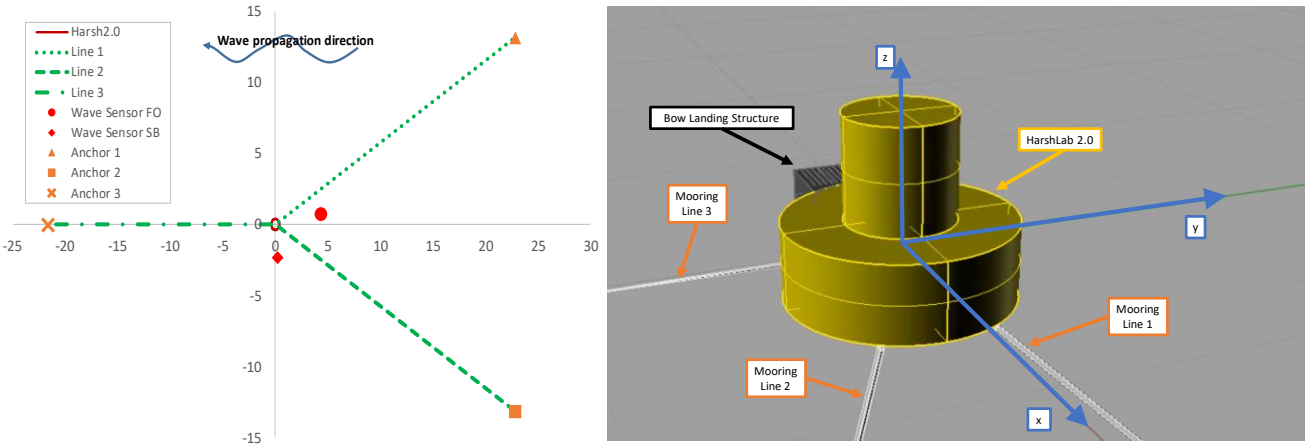

Figure 7 Mooring system representation of the Harsh 2.0 floating platform, scale 1:13.6. Mooring lines top view, HarshLab2.0 structure, mooring line anchors and wave sensor positions (left) and a representation of all structural components with the global coordinate system (right)

The mooring system properties of both the full scale and the scaled model are defined in Table 1 and Table 2:

Mooring Lines' anchor coordinates			***Mooring Lines' fairlead coordinates***		
Scale	**1:1**	**1:13.6**	**Scale**	**1:1**	**1:13.6**
x_{anchor} L1 [m]	310.59	22.84	$x_{fairlead}$ L1 [m]	4.53	0.33
y_{anchor} L1 [m]	179.32	13.19	$y_{fairlead}$ L1 [m]	2.62	0.19
z_{anchor} L1 [m]	-68.00	-5.00	$z_{fairlead}$ L1 [m]	-2.45	-0.18
x_{anchor} L2 [m]	310.59	22.84	$x_{fairlead}$ L2 [m]	4.53	0.33
y_{anchor} L2 [m]	-179.32	-13.19	$y_{fairlead}$ L2 [m]	-2.62	-0.19
z_{anchor} L2 [m]	-68.00	-5.00	$z_{fairlead}$ L2 [m]	-2.45	-0.18
x_{anchor} L3 [m]	-294.04	-21.62	$x_{fairlead}$ L3 [m]	-5.24	-0.39
y_{anchor} L3 [m]	0.00	0.00	$y_{fairlead}$ L3 [m]	0.00	0.00
z_{anchor} L3 [m]	-68.00	-5.00	$z_{fairlead}$ L3 [m]	-2.45	-0.18

Table 1 Mooring system anchor and fairleads for both scales

Mooring Lines Properies	
Variable	**Value (1:13.6)**
L1 length [m]	27.79
L2 length [m]	27.79
L3 length [m]	22.65
Equiv. Young Modulus [Pa]	3.35E+10
Bar diameter [m]	0.005
Equiv. A [m^2]	6.37E-05
Linear mass [kg/m]	0.5
Rayleigh Damp Coeff [-]	0.001
Seabed friction coeff [-]	0.5
Ca [-] (axial)	0.5
Ca [-] (radial)	1
Cd [-] (axial)	0.6389
Cd [-] (radial)	1.33
Hydrodynamic Diameter [m]	0.009

Table 2 Mooring line structural and hydrodynamic properties

Mooring system hydrodynamic properties have been taken from the reference [3] since isolated lines where characterized in wave basin. The axial stiffness has been taken from [10] and the Rayleigh damping coefficient, proportional to the axial stiffness, has been assumed.

Performed physical tests

Five sets of physical tests have been performed with different purposes as here detailed.

- Mooring stiffness tests (Table 3): The floating structure with the mooring has been given horizontal displacements in surge and sway to characterize the static properties of the mooring system
- Decay tests (Table 3): Two subsets of decay tests have been performed, first without the mooring system in the degrees of freedom with hydrostatic stiffness (heave, pitch and roll) and subsequently with mooring system in the degrees of freedom without hydrostatic force (surge, sway and yaw).
- Forced oscillatory tests (Table 4): Forced tests have been performed with several periods and amplitudes in surge, heave and pitch. Its objective has been to cover the most occurrent range and characterize the hydrodynamic radiation forces of the structure as well as the influence introduced by the attached structure representing the bow landing
- Regular wave tests (Table 5): A set of regular waves has been performed with different periods and one small amplitude to characterize the response amplitude operator (R.A.O.) of the moored structure
- Irregular wave tests (Table 6): A set of irregular wave tests has been performed in order to verify the moored model motions and mooring loads as well as to assess the numerical model applicability

Mooring Stiffnes tests	
Test nº	Heading [º]
1	0
2	30
3	45
4	90
5	135
6	180

Decay tests			
Test nº	Mooring	gree of freedo	Number of tests
1	no	roll	3
2	no	pitch	3
3	no	heave	3
4	yes	surge	3
5	yes	sway	3
6	yes	heave	3
7	yes	roll	3
8	yes	pitch	3
9	yes	yaw	3

Table 3 Mooring stiffness and decay tests lists

Forced oscillatory tests					
		Full Scale		1:13.6 Scale	
Test nº	DOF	Amplitude [m]	Period [s]	Amplitude [m]	Period [s]
1	surge / heave / pitch	0.4	16	0.03	4.34
2	surge / heave / pitch	0.6	16	0.04	4.34
3	surge / heave / pitch	0.8	16	0.06	4.34
4	surge / heave / pitch	0.4	14	0.03	3.80
5	surge / heave / pitch	0.6	14	0.04	3.80
6	surge / heave / pitch	0.8	14	0.06	3.80
7	surge / heave / pitch	0.4	12	0.03	3.25
8	surge / heave / pitch	0.6	12	0.04	3.25
9	surge / heave / pitch	0.8	12	0.06	3.25
10	surge / heave / pitch	0.4	10	0.03	2.71
11	surge / heave / pitch	0.6	10	0.04	2.71
12	surge / heave / pitch	0.8	10	0.06	2.71
13	surge / heave / pitch	0.4	8	0.03	2.17
14	surge / heave / pitch	0.6	8	0.04	2.17
15	surge / heave / pitch	0.8	8	0.06	2.17
16	surge / heave / pitch	0.4	6	0.03	1.63
17	surge / heave / pitch	0.6	6	0.04	1.63
18	surge / heave / pitch	0.8	6	0.06	1.63
19	surge / heave / pitch	0.4	4	0.03	1.08
20	surge / heave / pitch	0.6	4	0.04	1.08
21	surge / heave / pitch	0.8	4	0.06	1.08

Table 4 Performed forced oscillatory tests

Regular Wave tests				
	Full Scale		1:13.6 Scale	
Test nº	H [m]	T [s]	H [m]	T [s]
1	0.8	4.06	0.06	1.10
2	0.8	4.61	0.06	1.25
3	0.8	5.16	0.06	1.40
4	0.8	5.72	0.06	1.55
5	0.8	6.27	0.06	1.70
6	0.8	6.82	0.06	1.85
7	0.8	7.38	0.06	2.00

Table 5 Regular wave tests performed on the floating moored structure

Irregular Wave tests					
	Full Scale		Scale 1:13.6		
Test nº	Hs [m]	Tp [s]	Hs [m]	Tp [s]	gamma
1	1	5.79	0.07	1.57	1.4
2	1	7.72	0.07	2.09	1.5
3	1.36	9.65	0.1	2.62	1.8
4	1.88	6.87	0.14	1.86	1.4
5	1.88	9.15	0.14	2.48	1.5
6	1.88	11.44	0.14	3.1	1.8
7	3	7.79	0.22	2.11	1.4
8	3	10.39	0.22	2.82	1.5
9	3	12.98	0.22	3.52	1.8
10	5.6	9.22	0.41	2.5	1.6
11	4.3	12.29	0.32	3.33	1.9
12	2.04	14	0.15	3.8	1.8

Table 6 Performed Sea States (JONSWAP) in both the physical and numerical models

4 Results

The code has been validated through both decay tests and irregular wave simulations compared to wave tank tests. Simulations have been carried out in the time domain with the numerical model here presented based on linear hydrodynamics and non-linear lines dynamics model, as above introduced. Hydrodynamics of the structure has been performed with a linear wave interaction commercial code, ANSYS-AQWA [15]. The numerical wave interaction model of the submerged part has been built for the 1:13.6 scaled geometry, in which the cylindrical part of the structure has been modeled, without the attached bow landing shown in Figure 4, and whose radiation and diffraction coefficients are shown in Figure 8:

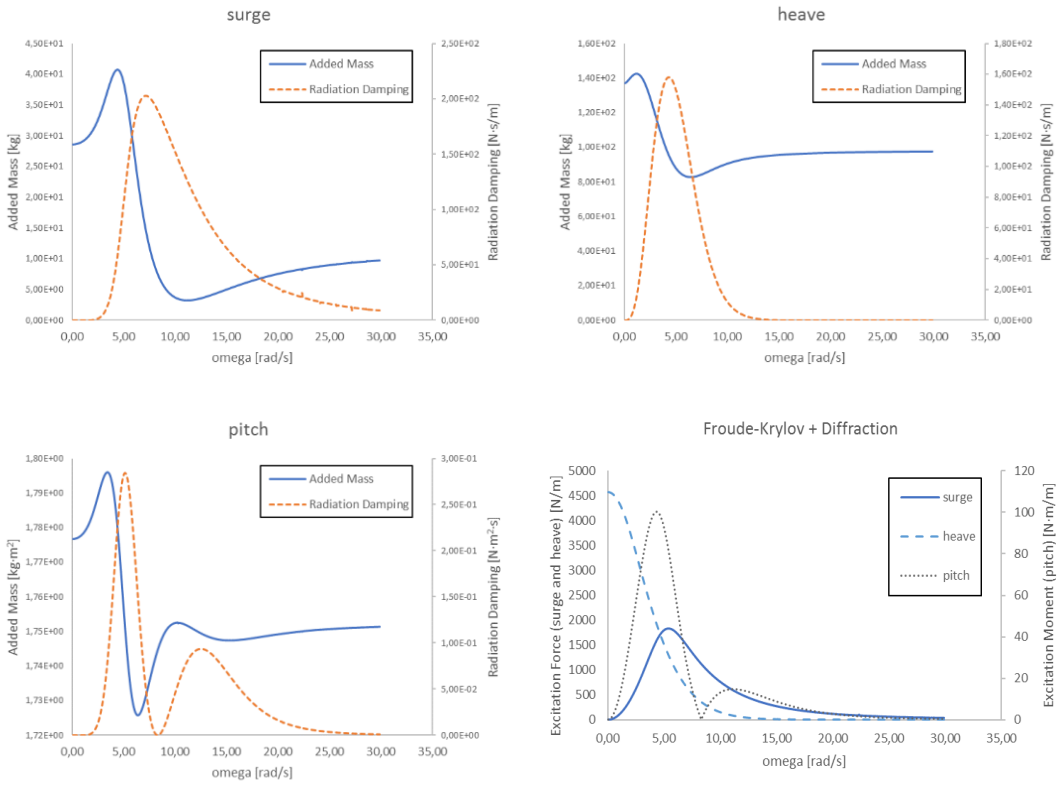

Figure 8 Hydrodynamic coefficients of the floating buoy HarshLab 2.0 in surge, heave and pitch. Added mass and Radiation damping of surge (top-left), heave (top-right) and pitch (bottom-left). Froude-Krylov and diffraction forces in surge, heave and pitch (bottom-right)

Due to the axisymmetric geometry of the numerical model no heave-pitch interaction is obtained from the linear potential code results. However, the attached structure for bow landing showed in Figure 4 couples the heave and pitch motions as well as the sway and yaw. Heave and pitch coupling has been accounted for through the Morison equation whilst the sway and yaw has not been fitted in this work since they are not significantly excited by the waves here analyzed.

The heave pitch coupling has been calculated from the pitching moment measured in the forced oscillatory tests in heave, introduced in Table 4. Three sets of forced tests, each of them with an amplitude and covering a relevant period range, have been utilized for that purpose. The measured moment has been fitted with the two factors of drag and inertia, as defined in (21).

$$(21)\, M_{5fit} = f_{d-53} \cdot \left|\dot{\delta}_3\right| \cdot \dot{\delta}_3 + f_{m-53} \cdot \ddot{\delta}_3$$

$$(22)\, M_{5bl} = -f_{d-53} \cdot \left|v_3 - \dot{\delta}_3\right| \cdot \left(v_3 - \dot{\delta}_3\right) + f_{m-53} \cdot \left(a_3 - \ddot{\delta}_3\right)$$

$$(23)\, F_{3bl} = -\frac{M_5}{x_{bl}}$$

Where the resulting mean fitted factors of the set showed in Figure 9 have been f_{d-53}=15.25 and $f_{m-53} = 1.698$. x_{bl} represents the distance from the center of gravity of the attached structure to the center of gravity of the whole structure, equal to 0.485m.

The overall influence of the attached bow landing structure in terms of drag, excitation and inertia effects have been introduced in the model ($F_{bl}(t)$ in equation (1)) through the Morison heave force and pitch moment as defined by (23) and (22) respectively. The viscous damping and hydrostatic stiffness introduced by the bow landing in each degree of freedom, additionally to the cross coupled already mentioned, has been assumed to have been included in the decay test viscous force fitting and the additional stiffness pointed out in Table 7, Table 8 and Table 10.

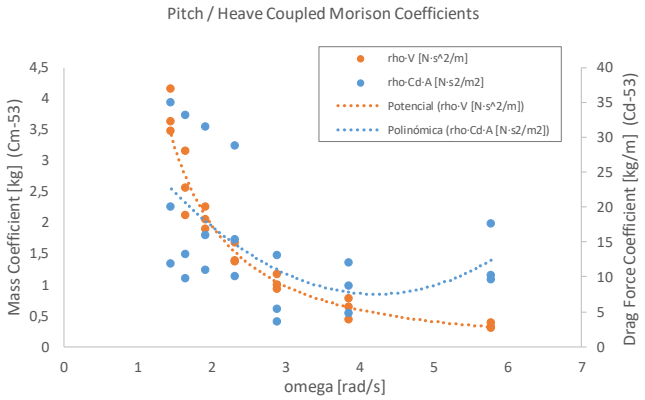

Figure 9 Heave-pitch cross coupling Morison coefficients

The validation of the code and hydrodynamic characterization has been broken down into four stages and presented in subsequent sections:

1- Drag coefficient numerical identification with decay tests of heave, pitch and roll without mooring system, specified in Table 3

2- Drag coefficient numerical identification with decay tests of surge, sway and yaw with mooring system, specified in Table 3

3- Simulation of the whole system imposing obtained motions of the structure in a set of irregular wave tests as defined in Table 6

4- Simulation of structure and mooring dynamics subject to waves excitation in the set of irregular sea states applied on the previous stage as defined in Table 6

The non-linear drag term of each degree of freedom 'j' in equation (20), is described by the equation (24):

$$(24)\, {F_{drag}}^{j} = C_j \cdot \left|u - \dot{\delta}_j\right| \cdot \left(u - \dot{\delta}_j\right)$$

The factor C_j is the corresponding factor identified in the decay tests for each degree of freedom. It has been applied only for translational degrees of freedom while only the velocity of the degree of freedom has been considered for rotational ones.

Decay tests without mooring system

The corresponding numerical model has been systematically simulated until the mean error compared with respect to the experimental decay test has been minimised. Even though the hydrostatic stiffness, accounting for the bow landing structure, should be accurately obtained with the physical model, it has not been available in this work. Therefore an added stiffness value to match the identified natural frequency has been added to the hydrostatic stiffness (Table 7), which has been assumed to be introduced by the bow landing.

The decay tests in the wave basin have been analysed to detect its damped natural frequency:

Dof	Nat Freq. (damped) [rad/s]	K added [%]	Damping Ratio [%]
heave	5,375	4,75	56,85%
roll	4,409	10,08	14,61%
pitch	4,330	6,21	30,12%

Table 7 Damped natural frequency identified from the decay tests and percentage of added stiffness in heave, pitch and roll due to the influence of the bow landing, present in the physical model

The drag coefficients and the corresponding error found after the mean quadratic error minimization are summarized in Table 8:

Dof	C (test 1)	C (test 2)	C (test 3)	C (mean)	error (test 1)	error (test 2)	error (test 3)
heave	626,68	795,47	1145,40	855,85	1,98E-07	2,50E-07	2,33E-07
roll	11,59	6,81	11,56	9,99	6,97E-06	5,95E-06	4,37E-06
pitch	30,40	14,29	16,75	20,48	3,14E-06	8,40E-07	1,39E-06

Table 8 Found drag force coefficients and the corresponding mean error for the three analyzed decay tests

Simulations of the decay tests show good approximations of the identified numerical model.

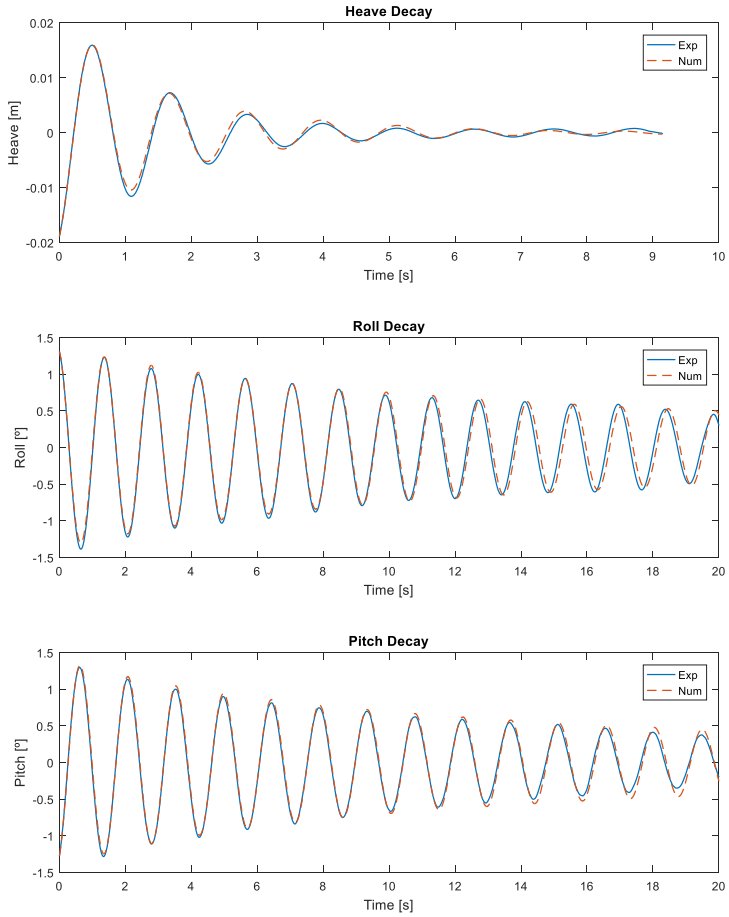

Figure 10 Decay test simulations after drag force coefficient computation in heave (top), roll (middle) and pitch (bottom)

It shows some differences in the tests after a significant decay of the motion probably due to changes in the viscous coefficient with significant differences of the Reynolds number.

Decay tests with mooring system

As carried out in the other degrees of freedom, sets of three decay tests have been analyzed to compute the corresponding drag force coefficients. In this case the mooring system is included whose lines have been modeled with 30 elements.

The mooring system static performance has been initially validated compared with the corresponding properties obtained in the wave tank. Mooring total forces in surge and heave with horizontal (positive x – surge) positions of the floating structure have been compared between the numerical and the physical models (Table 3) showing, in Figure 11, good agreement between both models. The static numerical model has been based on analytical catenary calculations [25] which also provides with initial conditions to the dynamic code here presented.

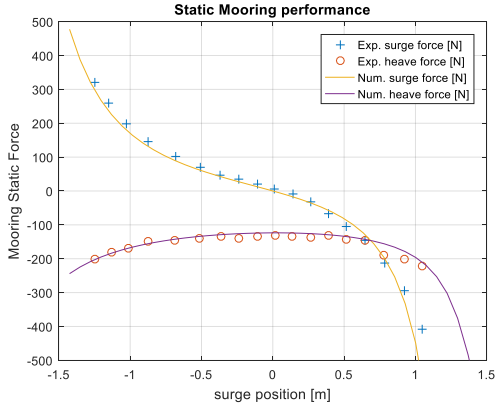

Figure 11 Static response of the mooring system to horizontal positions of the floating structure

Unlike in heave, roll and pitch no stiffness has been added to surge, sway and yaw since it is completely provided by the mooring system. Its identified natural frequencies are listed in Table 9:

Dof	Nat Freq. (damped) [rad/s]	Damping Ratio [%]
surge	0,993	35,42%
sway	0,489	67,86%
yaw	2,098	223,76%

Table 9 Damped natural frequencies identified in the decay tests in surge, sway and yaw

After mooring system static validation same subroutine has been used to compute drag force coefficients in surge sway and yaw as that applied for heave, roll and pitch. The corresponding values for the three decay tests as well as its errors are summarized in Table 10:

Dof	C (test 1)	C (test 2)	C (test 3)	C (mean)	error (test 1)	error (test 2)	error (test 3)
surge	75,23	83,16	64,91	74,43	1,56E-05	1,82E-05	2,39E-05
sway	77,89	71,00	61,20	70,03	7,63E-05	1,11E-04	1,01E-04
yaw	53,59	59,21	53,66	55,49	2,83E-05	2,19E-05	2,38E-05

Table 10 Found drag coefficients and the corresponding errors for each degree of freedom and decay test

Decay tests accounting for identified drag force coefficient included in the model are shown in Figure 12 and the corresponding line tension comparisons are plotted in Figure 13, Figure 14, and Figure 15 for surge, sway and yaw decay tests respectively.

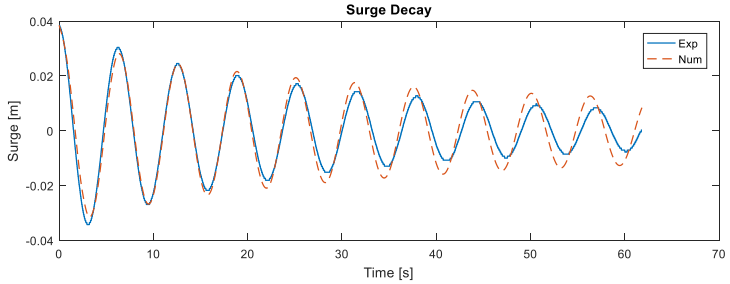

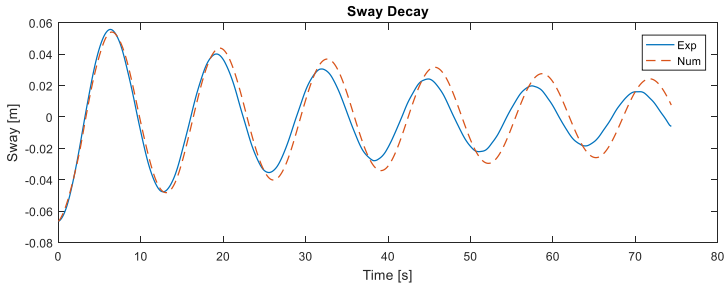

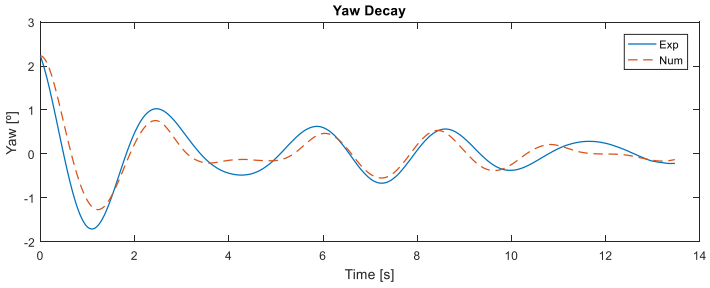

Figure 12 Decay test simulations after drag force coefficient computation in surge (top), sway (middle) and yaw (bottom

Floater dynamics have been found to be good compared to the experimental test cases. Natural frequencies are quite well identified, even though some differences are observed after four cycles in surge with a phase slightly lagged and after two cycles in sway with a little phase leading. Yaw decay is strongly non-linear since its stiffness is provided by fairleads rotation, effect which is appropriately caught representing well the interaction between line transverse dynamics and yaw of the structure. However, the influence of the inertia of some transverse mode of lines motions overestimated as shown at around second 4 in Figure 12 (bottom).

Line tensions in surge are slightly overestimated, especially for line 3, which may be influenced by the seabed interaction. The phase lag of the surging motion is also shown in the comparison of line tensions with the experimental decays.

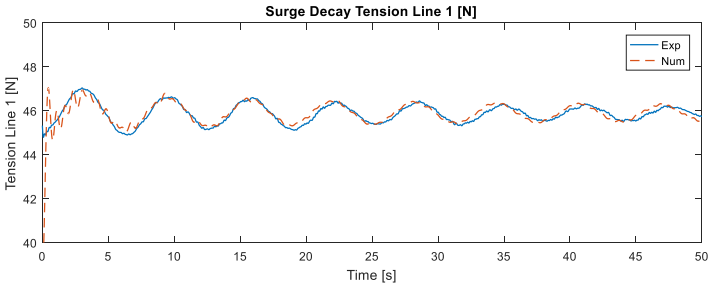

404

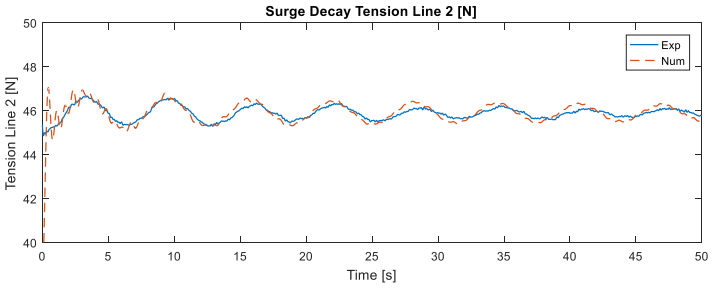

405

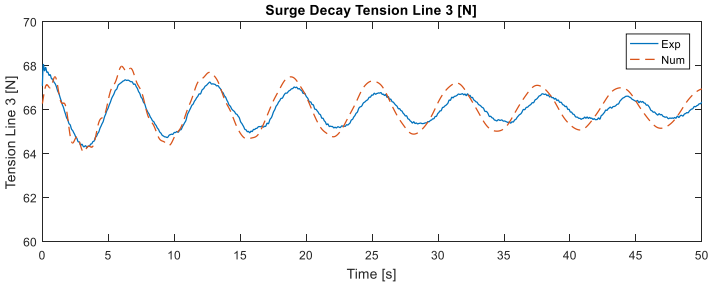

406

407 Figure 13 Line tension comparison between experimental and numerical models for decay tests in surge for the three lines

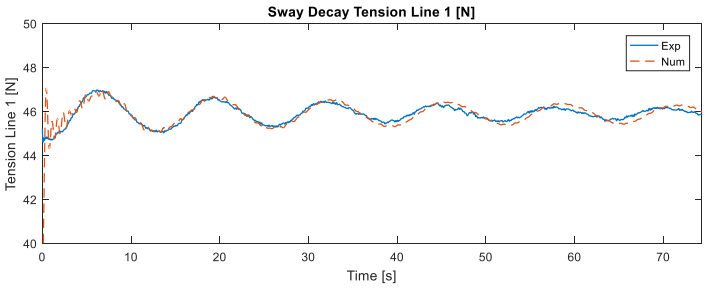

408

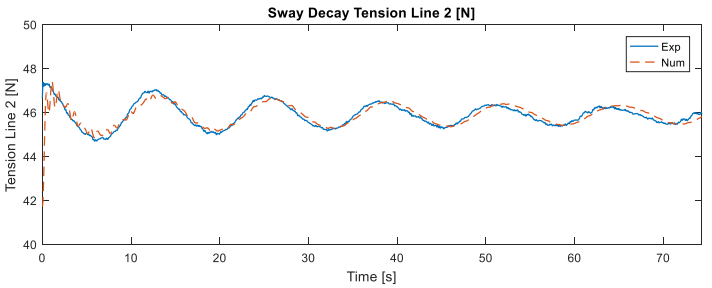

409

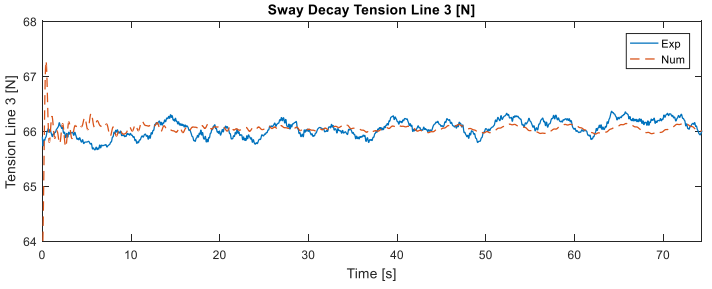

410

Figure 14 Line tension comparison between experimental and numerical models for decay tests in sway for the three lines

Results of the decays in sway show good agreement in lines 1 and 2 while line 3, since is most influenced by seabed friction, represent poorer performance. It is due to the very low tension induced by the fairlead transverse motion with a large influence of the seabed vertical force and horizontal friction. Same conclusions can be drawn for line tensions obtained with yaw decay tests, in Figure 15 for line 1, that shows the same performance as the other two lines. In this case a large period variation of the line tension is reproduced in the tests. It is likely due to a transverse mode of motion excitation not caught well or overdamped in the numerical model. It can therefore be expected poorer tension performance of lines exposed to significant fairlead transverse motions.

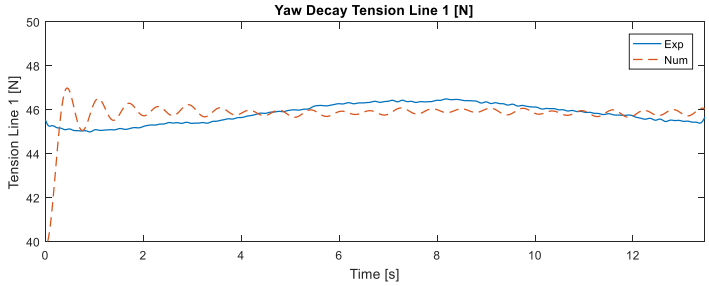

Figure 15 Line tension comparison between experimental and numerical models for decay tests in yaw for the three lines

All simulated cases have transitory line tensions due to the initial conditions, which have been set based on static catenary equations [19], [25]. Adjustments in section lengths make these initial line tensions to happen.

The heave and pitch coupling effects can be appreciated in the heave decay test with mooring and all the fitted drag coefficients included in the numerical model, as represented in Figure 16.

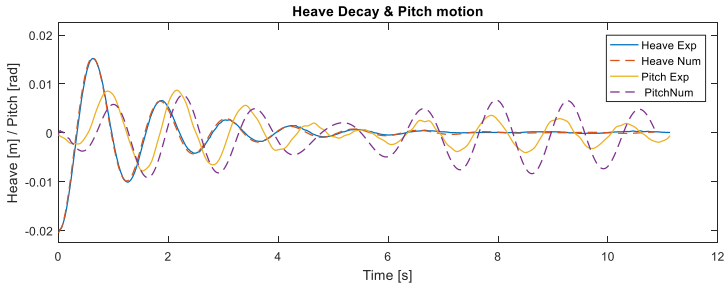

Figure 16 Heave decay test with mooring and the induced pitch motion. Solid lines: Experimental; Dashed lines: Numerical

It can be appreciated that the pitch motion with the mooring system included, after the decay of the heaving motion, is slightly underdamped and phase lagging. The fact of being underdamped also indicates that the excitation moment may also be underestimated as both effects come from the fitting introduced in Figure 9.

Imposed motions subject to irregular waves

Irregular wave experimental tests have been carried out for 12 irregular sea states, specified in Table 6.

In order to get the accuracy of the isolated mooring numerical model the experimental test motions have been imposed to the structure in the numerical model. These results set a basis to assess to what extent the error in line tensions is influenced by the mooring model and the hydrodynamic model.

Simulations show in general good agreement, obtaining even better accuracy compared with the decay test line tensions.

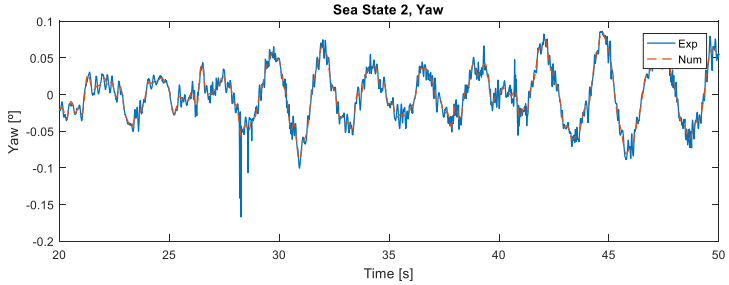

Figure 17 Obtained experimental model motion (Exp) and filtered imposed numerical motions (Num) in the Sea State 2

Even though the most excited motions (surge, heave and pitch) seem smooth enough to be directly imposed to the structure all signals have a significant noise from measuring sensors. That noise is amplified when derived to be applied to the numerical model which may be translated in artificial tension vibrations. To avoid that, a cut-off frequency of 30rad/s has been introduced to obtain smooth motions to be imposed, represented by a dashed line in Figure 17.

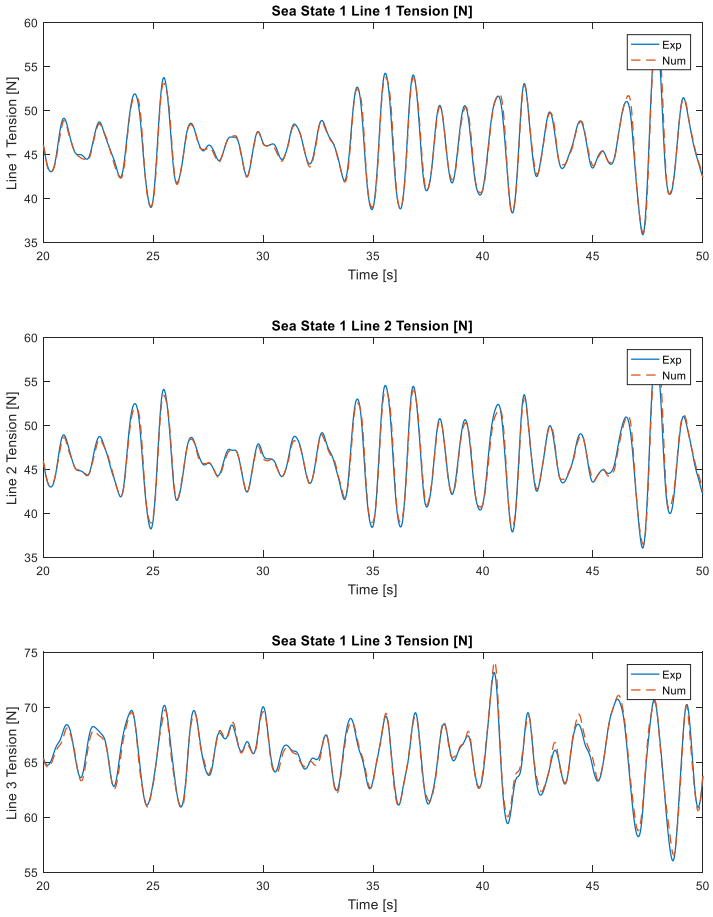

Figure 18 Line tensions obtained in the numerical simulations with imposed motions (dashed line) compared with the experimental tests in the Sea State 1 (solid line)

Both mean and dynamic tensions in Figure 18 show a very good agreement with the experimental line tensions. All sea states have been simulated in order to assess the error in the simulation, as represented in Figure 19 and Figure 20 for maximum line tensions and standard deviations respectively.

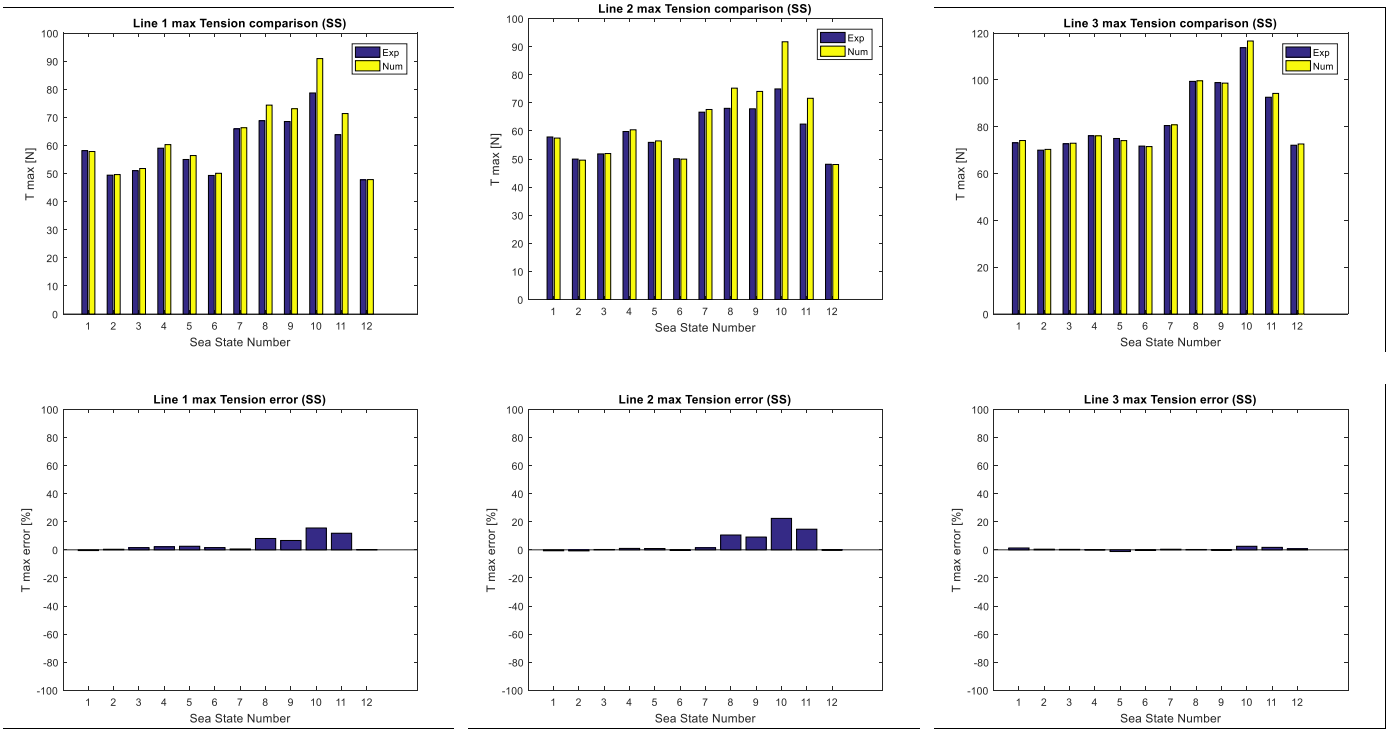

Figure 19 Maximum line tension comparisons (top) and maximum tension error percentages (bottom)

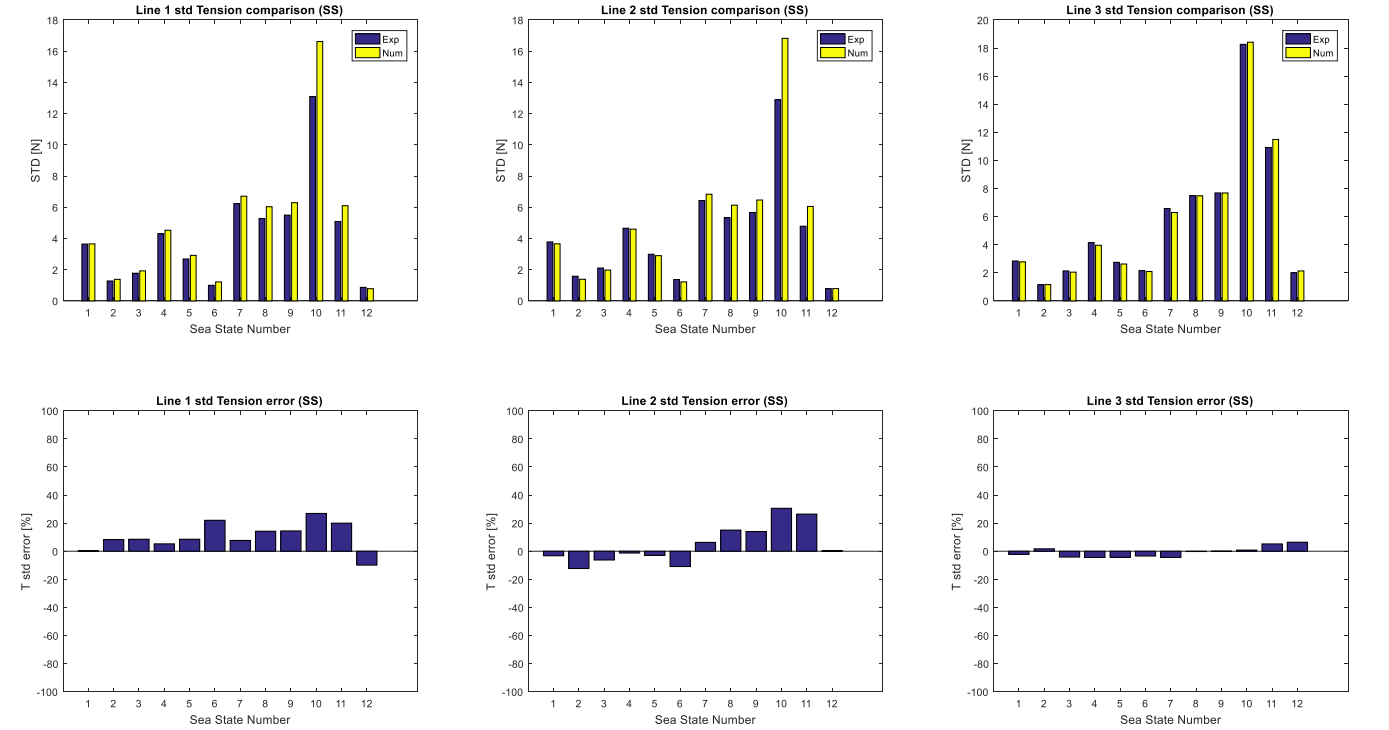

Figure 20 Standard deviations of line tension comparisons (top) and tension error percentages (bottom)

It can be observed that all errors for line 3 are well below 5% and 10% for maximum and standard deviations. However, lines 1 and 2 show larger errors very likely due to its transverse motions and more significant seabed interactions.

It is observed in Figure 20 that line 1 tension shows in general overpredicted standard deviations while line 2 underpredicts it under low energy sea states. This difference is well observed in sea state 6 with significant overprediction of line 1 and underprediction of line 2 of the numerical model.

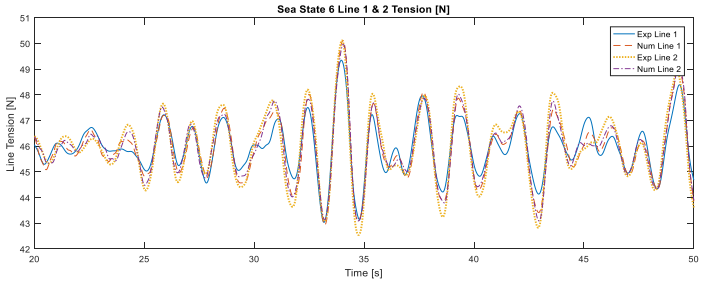

Figure 21 Lines 1 and 2 tensions from experimental and numerical tests

In Figure 21 slight differences are shown in the experimental line tensions, whilst the numerical model catches only partially such differences.

Even though the imposed transverse motions are well filtered the physical model seems to be much more sensitive to transverse motions of the structure, in terms of line tensions, compared to the numerical model. It is the main source of standard deviation difference between lines 1 and 2 compared to the physical model.

Structure and mooring dynamics subject to irregular waves

The last stage of the model validation consisted in fully non-linear simulation of dynamic moorings coupled with linear hydrodynamics as represented by equation (20). It represents a non-linear mooring system with non-linear anchor and fairlead relations with a linear hydrodynamic formulation.

In this case waves incoming from the positive ‘x’ axis, centered between lines 1 and 2 acting as windward lines and having line 3 as a leeward line, see Figure 7.

The wave elevation at the wave gauge has been based on SB measurements, as indicated in Figure 5, and corrected with the perpendicular distance to the structure, with the dispersion relation for deep waters, in the numerical model in order to carry out the simulations.

It should be considered that a regular wave amplitude of 5m in full scale corresponds to a Keulegan Carpenter (KC) number of 3. It means that the linear wave theory is applicable to almost all waves composing all sea states except some frequency components of sea states 7 to 11 where some disagreements may be due to slightly larger KC numbers.

Obtained numerical results for the sea state 1 are shown in Figure 22 and Figure 23 for the structure motions and line tensions respectively.

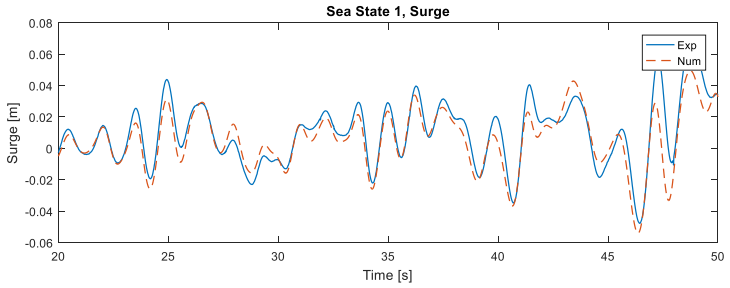

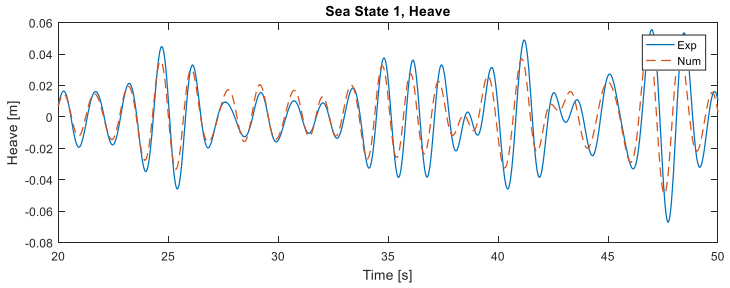

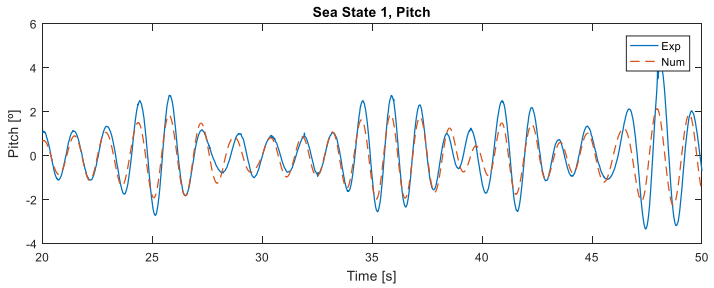

Figure 22 Relevant structure motions obtained in the hydrodynamics and mooring coupled simulation subject to sea state 1

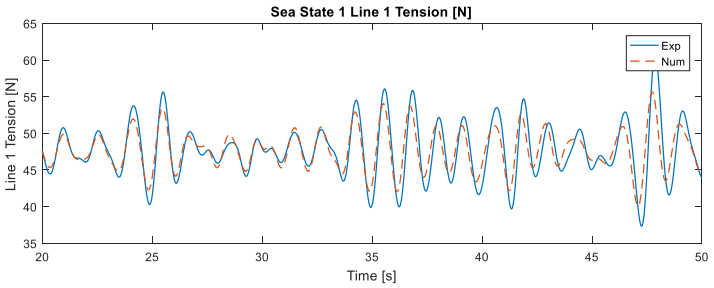

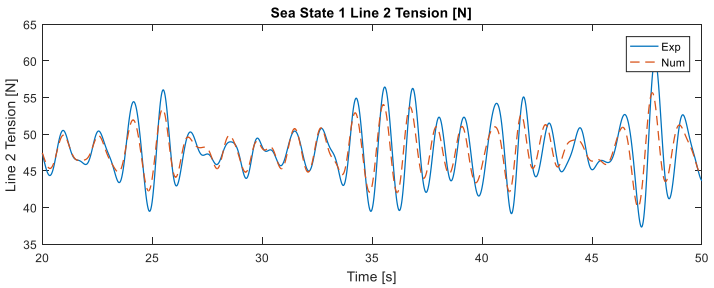

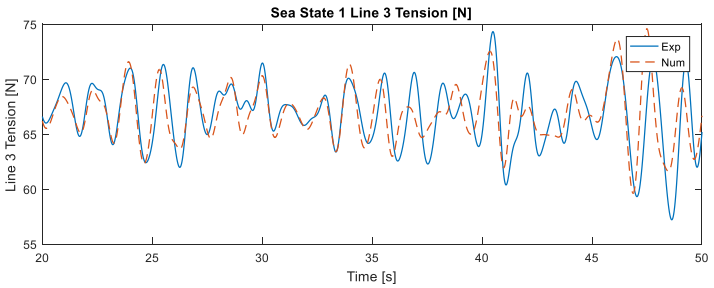

Figure 23 Lines tensions obtained in the hydrodynamics and mooring coupled simulations subject to sea state 1

After carrying out numerical simulations for the 12 sea states considered in this work a summary of results can be found in Figure 24, Figure 25 and Figure 26.

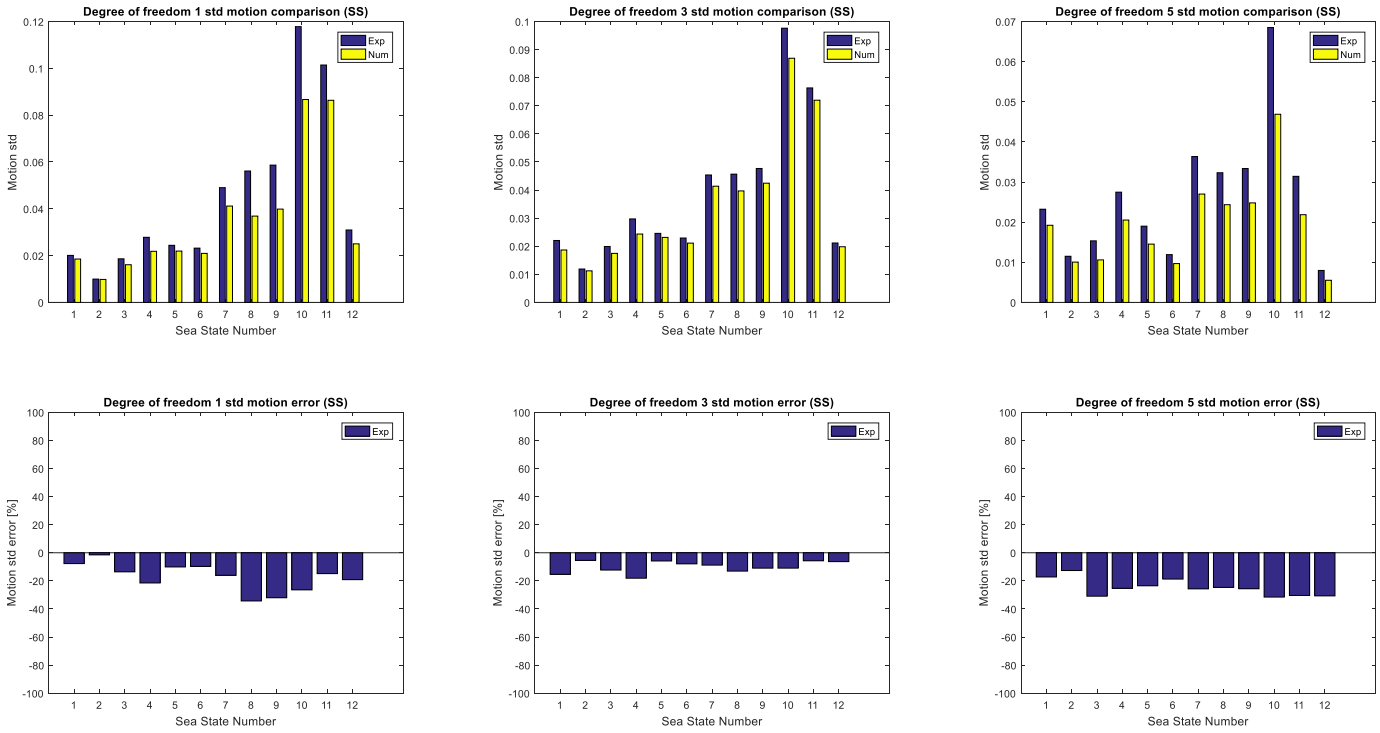

Figure 24 Structure motion standard deviations comparisons (top) and the corresponding error percentages (bottom). Degrees of freedom 1 (surge), 3 (heave) and 5 (pitch)

Structure motions are in general underpredicted. Whilst heave is very well reproduced with mean errors around 10% in standard deviation, surge and pitch motions show slightly larger errors. In the case of surge the errors may be mainly due to inaccuracies in mean and slowly varying drift force estimations, and especially sensitive to more energetic sea states, which is observed in Figure 23 (top). Pitch motion is the most underestimated motion with mean standard deviation errors of around 30%. It may probably be due to the changing submerged geometry with small pitch angles as pointed out by [6]. These errors may be improved implementing a non-linear hydrostatic stiffness force and/or excitation forces, as suggested in [20] and [26] respectively.

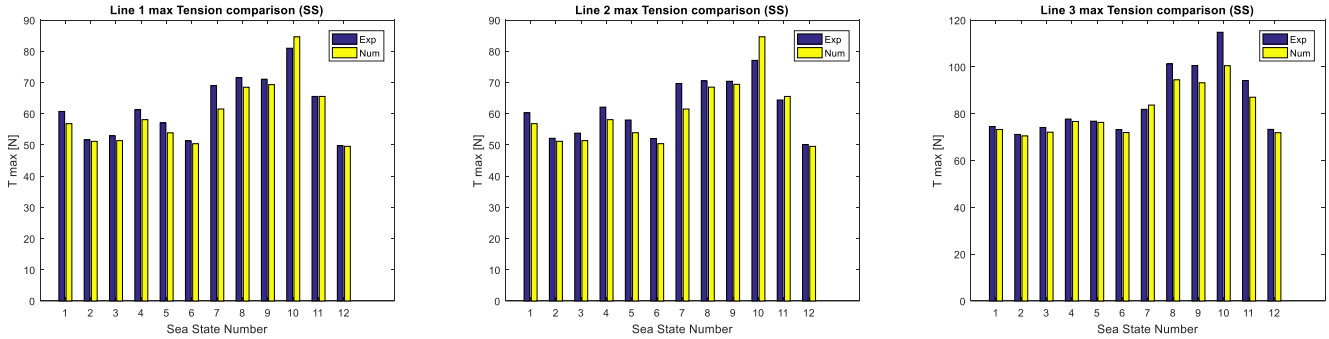

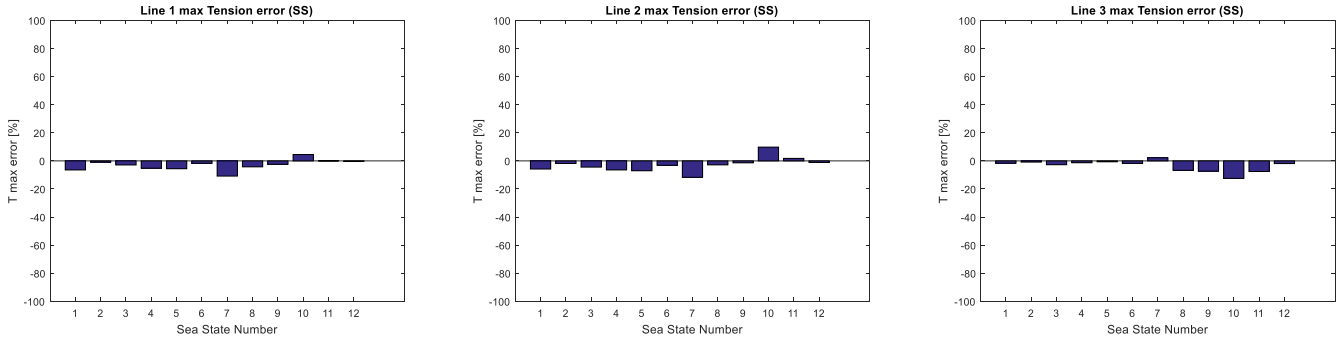

Figure 25 Maximum line tension comparisons (top) and error percentages (bottom) for hydrodynamics and mooring coupled simulations

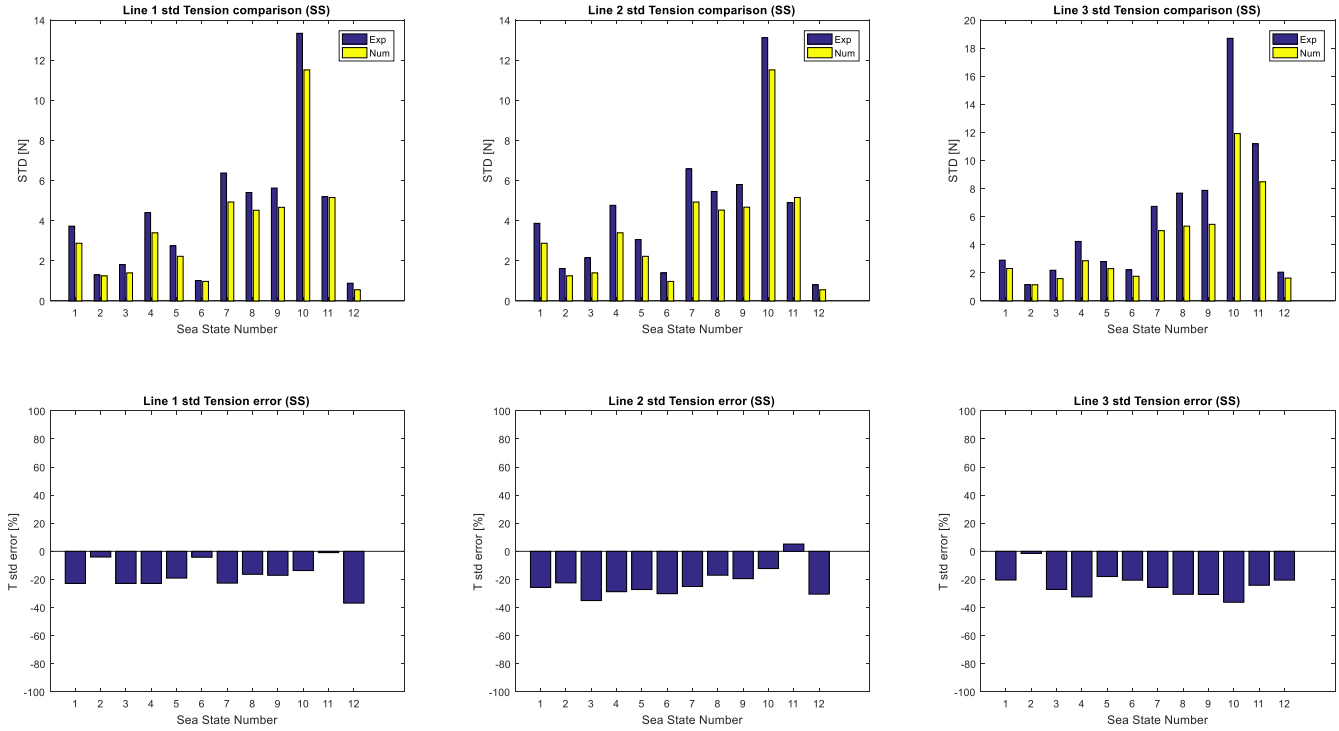

Figure 26 Standard deviations of line tensions (top) and their error percentage (bottom) for hydrodynamics and mooring coupled simulations

Simulations of linear hydro-lumped mass model still provide maximum line tensions with relative errors below 10% for lines 1 and 2, and below 5% for line 3. However, maximum line tensions are now underpredicted instead of being overpredicted as observed in the imposed motions simulations. Regarding standard deviations, the relative errors in line tensions are increased in absolute terms and in general underpredicted as a consequence of underpredicting in general body dynamics, specially pitching motions. In the case of lines 1 and 2 the underprediction appears to be less influenced in more energetic sea states. It is probably due to being balanced by the overprediction of the lumped mass model with imposed motions in those sea states. From a design perspective the most energetic sea states, such as 7 to 11 as specified in Table 6, are the most interesting for ultimate limit states. Even though these sea states show larger uncertainty in the presented results, the maximum line tensions show deviations of up to 10%, which are within the limits covered by the safety factors recommended by design standards. Additionally, the hydrodynamics of the structure may be completely defined by Morison coefficients fitted with tank tests for extreme conditions in order to improve the accuracy of the numerical model.

Discussion

Validation results have been broken down into four stages in order to identify sources of differences at each stage. Decay tests without mooring system show very good accuracy even with the influence of the bow landing. However, in order to have a good match of natural frequencies, a hydrostatic stiffness has been added which, in the physical model is supposed to having been introduced by the bow landing itself. In the moored decays some differences have been found both in phase and amplitude after 4 cycles in surge and 2 cycles in sway. That difference can be attributed to a mismatch of the added mass at infinite frequency with the physical model. Yaw decay is generally well caught, which is dominated by the mooring response. These disagreements in sway and yaw can be attributed to the coupling between yaw and sway, introduced by the bow landing in the physical model and not considered in the numerical model. The drag force coefficient identification seems to be feasible in all degrees of freedom as there is no large dispersion between tests of the same degree of freedom. It has also been shown that the transverse motion of the fairlead, as for line 3 in the sway decay and all lines in the yaw decay, leads to very high uncertainty in line tension estimation, possibly due to the seabed friction model.

Prescribed motions simulation has been carried out to set reference comparison of the mooring line tensions with the corresponding experimental results. Very good agreement has been found in terms of maximum line tension and good in terms of standard deviation. However, slightly larger differences have been obtained in windward lines probably due to having some transverse motion of the fairlead, which, as observed in the decay tests, can be attributed to the seabed friction model. Low sensitivity to sway, roll and yaw, compared to the physical model is observed as windward lines show larger tension differences in the physical model than in the numerical one.

Hydro-lumped mass simulations show very good agreement in heave whilst moderate in surge and pitch due to errors in slowly varying drift and non-linear stiffness/Froude-Krylov forces respectively. The underprediction is directly translated into line tensions, which in most energetic sea states may be balanced by the overprediction of the imposed motions simulations. Obtained line tension errors with respect to the experimental tank tests are aligned with the suggested safety factors, generally around 1.5 only for dynamic tension, which is conservative compared with the results here presented.

5 Conclusions

In this paper a non-linear dynamic lumped mass numerical model has been presented to assess mooring lines performance along with floating body dynamics based on linear potential theory with identified viscous drag terms. Both are related by kinematic relations, reduced to a set of stiffness, damping and mass matrices which are solved together considered as a single mechanical multi-degree of freedom system. The time resolution is carried out by means of the Newmark method since the resulting numerical model is a stiff system.

The validation and fitting of the numerical model has been done based on the HarshLab 2.0 tank tests of a 1:13,6 scaled physical model, which is a CALM buoy with an attached bow landing. The structure is moored with three chain catenary lines.

The validation procedure has been broken down into four stages, decay tests without and with mooring system, imposed motions and the floater wave interaction model coupled to the lumped mass model simulations.

The influence of the bow landing has been modelled introducing an added numerical stiffness in heave, roll and pitch. Due to its position a heave-pitch and sway-yaw coupling is also introduced in the physical model. The former has been modelled from forced oscillation tests whilst the latter has not been modelled since it has been supposed not to be relevant for the present work. Additionally, its viscous drag is supposed to be included in the identified drag coefficient for each degree of freedom.

Prescribed motion simulations show disagreements in maximum line tension of up to 20% in the windward lines, the leeward line, aligned with wave direction, shows differences of up to 5%. Windward lines' differences, having a partially transverse motion, may be attributed to the seabed friction model. However, to get a convincing conclusion that the discrepancy is due to the friction model, a further study in the influence of friction models should be conducted. Standard deviations show a larger sensitivity of the physical model to very small transverse oscillations of the structure (i.e. sway, roll and yaw) compared with the numerical model. It shows differences of up to 20% in standard deviations between both leeward lines, which are initially expected to be insignificant. Slight overprediction of lines tensions is observed in most energetic sea states for all lines, affecting especially to lines 1 and 2 and having almost an insignificant impact on line 3.

Hydro-lumped mass model simulations catches well the device performance in general. However, structure motions are underpredicted. While heaving motions show reduced errors, largest uncertainties come from surge and pitch motions. Surge motions seem to be underestimating slowly varying drift forces. Pitch motions underestimation is the most critical source of uncertainty, very likely due to non-linear hydrostatic stiffness and Froude-Krylov forces. The underprediction is translated to line tensions which may be slightly balanced by the overprediction of the imposed motions subject to energetic sea states. Even though the disagreements in structure dynamics, the leeward line, aligned with the wave propagation direction, almost keeps its accuracy with respect to the prescribed motion simulations, with maximum line tension difference lower than 5%.

The coupled model appears to be a feasible way of modelling both dynamic systems coupled into a single one. Even though the resulting system is stiff and requires a small time-step, the simulation does not require two solvers to be solving in parallel.

Results show very good agreement in general for imposed motions simulations and accurate enough in the coupled simulations, compared with suggested safety factors in offshore standards in terms of line tensions [27].

Non-linear assessment of hydrostatics and excitation forces along with a deeper analysis of the bow landing and seabed properties influence should lead to improvements on the coupled results.

Authors are currently working on a linearized coupled system to account for line dynamics in the frequency domain. Such models may be useful for efficient fatigue assessment of mooring lines.

6 Acknowledgments

HarshLab was partly funded by i) Basque Government through the Project HAZITEK 2016-HARSH (ZE-2016/00017) and through two direct grants (exp. 2017/00927) (A/2017/0277) and (EXP. 2018/01144) (A/20180397); and ii) Ente Vasco de la Energía (EVE), through the «Programa de ayudas a la Demostración y Validación de Tecnologías Energéticas Renovables Marinas (MARINA 2016 002)»

Funded by Project IT949-16 given by the Departamento de Educación, Política Lingüística y Cultura of the Regional Government of the Basque Country.

Funded by the Spanish Government through the Ministerio de Economía y Competitividad (Project DPI2015-67626-P (MINECO/FEDER, UE)).

7 References

[1] V. D. Boom and H. J.j, "Dynamic behaviour of mooring lines," *Marit. Res. Inst. Neth. Mar. Wagening. Behav. Offshore Struct. Elsevier Sci. Publ. BV Amst. Neth. Pap. P1985-10 Proc.*, 1985.

[2] M. Hall and A. Goupee, "Validation of a lumped-mass mooring line model with DeepCwind semisubmersible model test data," *Ocean Eng.*, vol. 104, pp. 590–603, Aug. 2015, doi: 10.1016/j.oceaneng.2015.05.035.

[3] J. Azcona, X. Munduate, L. González, and T. A. Nygaard, "Experimental validation of a dynamic mooring lines code with tension and motion measurements of a submerged chain," *Ocean Eng.*, vol. 129, pp. 415–427, Jan. 2017, doi: 10.1016/j.oceaneng.2016.10.051.

[4] V. Harnois *et al.*, "Numerical model validation for mooring systems: Method and application for wave energy converters," *Renew. Energy*, vol. 75, pp. 869–887, Mar. 2015, doi: 10.1016/j.renene.2014.10.063.

[5] K. Xu, Z. Gao, and T. Moan, "Effect of hydrodynamic load modelling on the response of floating wind turbines and its mooring system in small water depths," *J. Phys.*, p. 15.

[6] T. H. J. Bunnik, G. de Boer, J. L. Cozijn, J. van der Cammen, E. van Haaften, and E. ter Brake, "Coupled Mooring Analysis and Large Scale Model Tests on a Deepwater Calm Buoy in Mild Wave Conditions," presented at the ASME 2002 21st International Conference on Offshore Mechanics and Arctic Engineering, 2009, pp. 65–76, doi: 10.1115/OMAE2002-28056.

[7] J. Azcona, D. Palacio, X. Munduate, L. González, and T. A. Nygaard, "Impact of mooring lines dynamics on the fatigue and ultimate loads of three offshore floating wind turbines computed with IEC 61400-3 guideline: Impact of mooring lines dynamics on the fatigue and ultimate loads of three offshore floating wind turbines computed with IEC 61400-3 guideline," *Wind Energy*, vol. 20, no. 5, pp. 797–813, May 2017, doi: 10.1002/we.2064.

[8] "Strength assessment of offshore structures - Sesam," *DNV GL*. [Online]. Available: https://www.dnvgl.com/services/strength-assessment-of-offshore-structures-sesam-software-1068. [Accessed: 15-Dec-2019].

[9] D. Gl, "SIMA Coupled Motion Analysis, Wind Turbines," p. 26, 2018.

[10] "OrcaFlex - dynamic analysis software for offshore marine systems," *Orcina*. [Online]. Available: https://www.orcina.com/orcaflex/. [Accessed: 15-Dec-2019].

[11] Z. Ran, M. H. Kim, and W. Zheng, "Coupled Dynamic Analysis of a Moored Spar in Random Waves and Currents (Time-Domain Versus Frequency-Domain Analysis)," *J. Offshore Mech. Arct. Eng.*, vol. 121, no. 3, pp. 194–200, Aug. 1999, doi: 10.1115/1.2829565.

[12] "BiMEP." [Online]. Available: https://bimep.com/pages/info. [Accessed: 19-Dec-2019].

[13] "Home," *HarshLab*. [Online]. Available: https://harshlab.eu/. [Accessed: 19-Dec-2019].

[14] "Wamit, Inc. - The State of the Art in Wave Interaction Analysis." [Online]. Available: https://www.wamit.com/. [Accessed: 19-Dec-2019].

[15] "ANSYS Aqwa | Hydrodynamics Simulation & Diffraction Analysis." [Online]. Available: https://www.ansys.com/products/structures/ansys-aqwa. [Accessed: 19-Dec-2019].

[16] S. Jamet, "NEMOH-Presentation," *LHEEA*. [Online]. Available: https://lheea.ec-nantes.fr/logiciels-et-brevets/nemoh-presentation-192863.kjsp?RH=1489593406974. [Accessed: 19-Dec-2019].

[17] J. Garcia De Jalon, *Kinematic and dynamic simulation of multibody systems: the realtime challenge.* Place of publication not identified: Springer, 2012.

[18] W. E. Cummins, "The Impulse Response Function and Ship Motions," Feb. 2010.

[19] "Sea loads ships and offshore structures | Engineering design, kinematics, and robotics | Cambridge University Press." [Online]. Available: https://www.cambridge.org/es/academic/subjects/engineering/engineering-design-kinematics-and-robotics/sea-loads-ships-and-offshore-structures?format=PB&isbn=9780521458702. [Accessed: 19-Dec-2019].

[20] F. Wendt *et al.*, "Ocean Energy Systems Wave Energy Modelling Task: Modelling, Verification and Validation of Wave Energy Converters," *J. Mar. Sci. Eng.*, vol. 7, no. 11, p. 379, Nov. 2019, doi: 10.3390/jmse7110379.
[21] K. Nielsen *et al.*, "OES Task 10 WEC heaving sphere performance modelling verification," p. 7.
[22] O. A. Maestre, A. H. Frías, E. A. S. Martín, and V. P. Arcocha, "Parámetros redundantes para Rotación y Traslación en Cinemática," p. 8.
[23] "DNV-RP-C205: Environmental Conditions and Environmental Loads," p. 124, 2010.
[24] A. Naess and T. Moan, "Stochastic Dynamics of Marine Structures," *Cambridge Core*, Oct-2012. [Online]. Available: /core/books/stochastic-dynamics-of-marine-structures/DFAC38B95E3AF664297DE6792524A4E2. [Accessed: 19-Dec-2019].
[25] I. Touzon, B. de Miguel, V. Nava, V. Petuya, I. Mendikoa, and F. Boscolo, "Mooring System Design Approach: A Case Study for MARMOK-A Floating OWC Wave Energy Converter," presented at the ASME 2018 37th International Conference on Ocean, Offshore and Arctic Engineering, 2018, doi: 10.1115/OMAE2018-77634.
[26] M. Penalba, A. Mérigaud, J.-C. Gilloteaux, and J. V. Ringwood, "Influence of nonlinear Froude–Krylov forces on the performance of two wave energy points absorbers," *J. Ocean Eng. Mar. Energy*, vol. 3, no. 3, pp. 209–220, Aug. 2017, doi: 10.1007/s40722-017-0082-x.
[27] "DNVGL-OS-E301.pdf." .